

# Production of ultracold $^{87}\text{Rb}^{133}\text{Cs}$ in the absolute ground state: complete characterisation of the STIRAP transfer

Peter K. Molony <sup>\*</sup>   Philip D. Gregory <sup>\*</sup>   Avinash Kumar <sup>\*</sup>   C. Ruth Le Sueur <sup>†</sup>  
Jeremy M. Hutson <sup>†</sup>   Simon L. Cornish <sup>\*‡</sup>

## Abstract

We present the production of ultracold  $^{87}\text{RbCs}$  molecules in the electronic, rovibrational and hyperfine ground state, using stimulated Raman adiabatic passage to transfer the molecules from a weakly bound Feshbach state. We measure one-way transfer efficiencies of 92(1)% and fully characterise the strengths and linewidths of the transitions used. We model the transfer, including a Monte Carlo simulation of the laser noise, and find this matches well with both the transfer efficiency and our previous measurements of the laser linewidth and frequency drifts.

## 1 Introduction

Ultracold dipolar molecules are currently a topic of intense research [1, 2], motivated by the presence of a permanent electric dipole moment which causes anisotropic, long range interactions which can be tuned by external electric fields [3]. The precise control possible with ultracold systems offers exciting prospects in quantum computation [4], quantum simulation [5, 6], precision measurements [7, 8, 9] and quantum-controlled chemistry [10, 11]. Direct laser cooling of molecules is beginning to show results [12, 13, 14], and recent work with microwave rotational cooling [15] and Sisyphus cooling [16] may lead to large trapped samples. However, none of these techniques are currently close to achieving the sub- $\mu\text{K}$  temperatures often found in cold-atom experiments.

For reaching sub- $\mu\text{K}$  temperatures, the most successful approach so far is to associate ultracold atoms to form weakly bound molecules by tuning an applied magnetic field across a zero-energy Feshbach resonance [17, 18], followed by transfer to the ground state by stimulated Raman adiabatic passage (STIRAP) [19]. Several groups have had success with homonuclear alkali molecules [20, 21, 22], but these have no dipole moment in the ground state, so considerable work is focussed on making heteronuclear molecules. Pioneering experiments with  $^{40}\text{K}^{87}\text{Rb}$  molecules have led to a series of exciting studies in quantum state-controlled chemistry [10], spin-lattice models [23] and strongly interacting many-body dynamics [24]. However, ground-state KRb molecules are energetically unstable because the exchange reaction  $2\text{KRb} \rightarrow \text{Rb}_2 + \text{K}_2$  is exothermic [10], and this leads to fast molecule loss [25] unless the molecules are protected in the collision-free environment of an optical lattice [23].

More recently, nonreactive  $^{87}\text{RbCs}$  molecules have been produced, both by our group [26] and by Takekoshi *et al.* [27]. Bosonic  $^{87}\text{RbCs}$  offers a contrast to fermionic KRb, and the large dipole moment of  $d_0 = 1.225 \text{ D}$  can be aligned to the laboratory frame with relatively modest electric fields to give  $d_0/3$  at a field of  $E_{\text{crit}} = 0.9 \text{ kV cm}^{-1}$  [26]. Other nonreactive ground-state molecules have been made very recently: Park *et al.* have made  $^{23}\text{Na}^{40}\text{K}$  [28] and Guo *et al.* have made  $^{23}\text{Na}^{87}\text{Rb}$  [29].

---

<sup>\*</sup>Joint Quantum Centre (JQC) Durham-Newcastle, Department of Physics, Durham University, South Road, Durham DH1 3LE, United Kingdom

<sup>†</sup>Joint Quantum Centre (JQC) Durham-Newcastle, Department of Chemistry, Durham University, South Road, Durham, DH1 3LE, United Kingdom

<sup>‡</sup>Corresponding author, s.l.cornish@durham.ac.uk

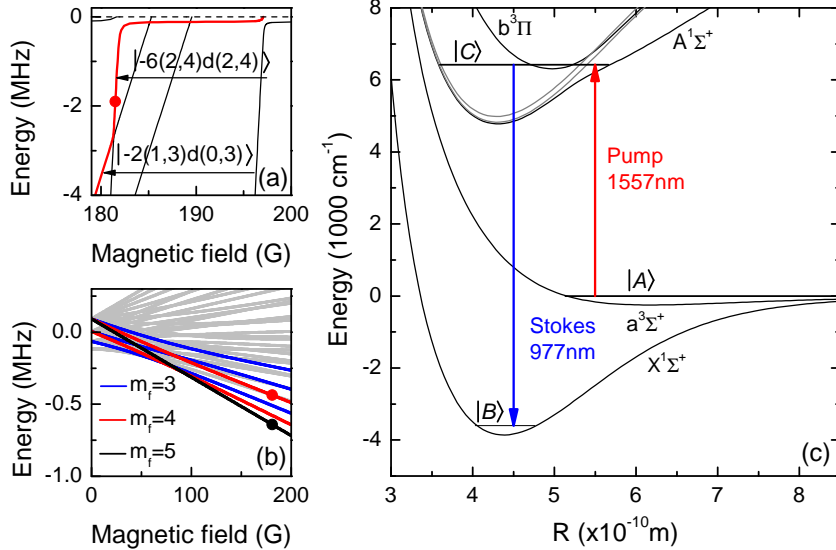


Figure 1: Molecular potentials and states used for transfer to the absolute ground state. (a) Zeeman structure of the initial weakly bound Feshbach states. The highlighted state shows the path followed by the molecules directly after magnetoassociation at the Feshbach resonance at 197.10(3) G. The states are labelled  $|n(f_{\text{Rb}}, f_{\text{Cs}})L(m_{f_{\text{Rb}}}, m_{f_{\text{Cs}}})\rangle$  as explained in the text. The dot shows the initial state and magnetic field for STIRAP. (b) Zeeman structure of the final state, showing the hyperfine structure of  $^{87}\text{RbCs}$  in the rovibrational ground state. Selection rules allow us to address only the highlighted states. The black dot shows the final state we address, which we note is the absolute ground state at this field. (c) Molecular potentials for  $^{87}\text{RbCs}$ , showing the laser wavelengths used in the STIRAP transfer.

In all of these experiments, it is essential to understand and model the STIRAP process, to obtain the most efficient transfer to the ground state. In the simplest form, STIRAP can be modelled analytically from a three-level Hamiltonian [30]. However, this does not account for the finite lifetime of the intermediate state, or the effects of laser noise, and both affect the efficiency of the transfer process.

In this article, we build a model of the transfer including the effects of finite laser linewidth, based on [31], and find excellent agreement with experimental measurements of the STIRAP transfer and independent measurements of the laser linewidth and shot-to-shot noise [32]. We also completely characterise the transitions used in the transfer with direct measurements of the Rabi frequencies, and we estimate the excited-state lifetime. This gives a simple, well understood route for the creation of ground-state  $^{87}\text{RbCs}$  molecules and a valuable diagnostic for optimising the laser system. With these improvements, we are able to achieve one-way transfer efficiencies of 92(1)% to the rovibrational and hyperfine ground state, surpassing our previous results [26].

## 2 Preparation of Feshbach molecules

We start our association from a precooled sample of  $^{87}\text{Rb}$  and  $^{133}\text{Cs}$  in a levitated optical trap ( $\lambda = 1550$  nm) in the  $|f = 1, m_f = 1\rangle$  and  $|3, 3\rangle$  states respectively. Typically the gas consists of  $\sim 3 \times 10^5$  of each species at  $\sim 300$  nK. Details of our apparatus and cooling method can be found in our previous publications [33, 34, 35]. We produce weakly bound molecules on the Feshbach resonance at 197 G and use Stern-Gerlach separation in the  $|-2(1, 3)d(0, 3)\rangle$  state at 181 G to remove the unbound atoms, as has been documented in [36]. This leaves up to 5000 Feshbach molecules confined in a levitated optical trap with a lifetime of 0.21(1) s. We detect the Feshbach molecules by dissociating them into atoms and taking a pair of absorption images at

low field using resonant light for Rb and Cs. As in [26], the weakly bound states populated by Feshbach association are labelled as  $|n(f_{\text{Rb}}, f_{\text{Cs}})L(m_{f_{\text{Rb}}}, m_{f_{\text{Cs}}})\rangle$ , where  $n$  is the vibrational label for the particular hyperfine ( $f_{\text{Rb}}, f_{\text{Cs}}$ ) manifold, counting down from the least-bound state which has  $n = -1$ , and  $L$  is the quantum number for rotation of the two atoms about their center of mass. All states have  $M_{\text{tot}} = 4$ , where  $M_{\text{tot}} = M_F + M_L$  and  $M_F = m_{f_{\text{Rb}}} + m_{f_{\text{Cs}}}$ . These states are shown in figure 1(a).

The  $|-2(1, 3)d(0, 3)\rangle$  state has poor coupling to electronic excited states of the molecule. For STIRAP we therefore transfer the molecules into the  $|-6(2, 4)d(2, 4)\rangle$  state which has much stronger coupling. However, this state is weak-field-seeking with a magnetic moment of  $1.5 \mu_B$  and cannot be magnetically levitated with our current coil setup. We therefore increase the trapping power in 7 ms to  $\sim 1$  W per beam and then turn off the magnetic gradient in 0.5 ms. This leaves up to 4000 molecules at  $1.5(2) \mu\text{K}$  in an all-optical potential which can trap any state. Finally we increase the bias field to  $181.624(1)$  G while the gradient switches off, transferring the molecules to the  $|-6(2, 4)d(2, 4)\rangle$  state which is the starting point for our ground-state transfer and all subsequent work in this paper.

### 3 Transfer to the ground state

Transfer to the ground state via STIRAP relies on a dark state  $|\psi\rangle$  that is an eigenstate of the Hamiltonian of a  $\lambda$ -type system on two-photon resonance. This is composed of a superposition of the initial Feshbach state  $|A\rangle$  and the final ground state  $|B\rangle$ , as shown in figure 1(c),

$$|\psi\rangle = \cos\theta|A\rangle + \sin\theta|B\rangle \quad (1)$$

where the exact composition is determined by the ratio of the pump and Stokes Rabi frequencies ( $\Omega_{\text{P}}$  and  $\Omega_{\text{S}}$  respectively) by the relationship

$$\tan\theta = \Omega_{\text{P}}/\Omega_{\text{S}} \quad (2)$$

This superposition is mediated by the excited state  $|C\rangle$  which in our case quickly decays if populated. Transfer from state  $|A\rangle$  to  $|B\rangle$  is then achieved by adiabatically ramping  $\Omega_{\text{P}}$  up and  $\Omega_{\text{S}}$  down, causing an adiabatic change in the mixing angle  $\theta$  from  $0 \rightarrow \pi/2$ . Crucially, the lossy excited state  $|C\rangle$  is never populated. We neglect the finite lifetime of the Feshbach and ground states because they are long on the timescale of the STIRAP transfer.

It has been shown [31] that a necessary condition for transfer is

$$\frac{\Omega_0^2}{\pi^2\Gamma} \gg \frac{1}{\tau} \gg W. \quad (3)$$

Here  $W$  is the linewidth associated with the frequency difference between the lasers,  $\tau$  is the transfer time,  $\Gamma$  is the excited-state decay rate, and  $\Omega_0 = \sqrt{\Omega_{\text{P}}^2 + \Omega_{\text{S}}^2}$ . This reveals two conditions: the transfer must be adiabatic, i.e., slower than the characteristic rate  $\Omega_0^2/\pi^2\Gamma$ , and the lasers must have a long coherence time. Thus we need two narrow-linewidth lasers, and an excited state with a long lifetime and high transition strengths to both the initial and final states.

A full description of our laser system for STIRAP has been presented elsewhere [32]. Briefly, a pair of external cavity diode lasers at 1557 nm and 977 nm supply the light for STIRAP. These are stabilised to a single optical cavity with a finesse of  $\sim 1.2 \times 10^4$ . The cavity is constructed from ultra-low-expansion glass, mounted in a vacuum chamber and stabilised to  $35^\circ\text{C}$ , the zero-crossing of the thermal expansion coefficient. Fibre-coupled electro-optic modulators provide continuous tuning of the laser frequencies, while high-speed Pound-Drever-Hall feedback loops narrow the linewidths [37]. We focus up to 16 mW of each wavelength to waists of  $37.7(1) \mu\text{m}$  (pump) and  $35.6(6) \mu\text{m}$  (Stokes) at the molecule sample. In our earlier publication [32], we measured the short-term linewidth of the 1557 nm laser to be  $0.52(2)$  kHz and a frequency drift of  $\sim 100$  kHz over the few hours it normally takes to map out the transfer as in figure 2. The 977 nm laser system is identical, so it is reasonable to assume it has similar noise characteristics.

Figure 1(c) shows the initial and final states for our transfer, and the transitions at 1557 nm and 977 nm within the molecular potentials. We choose as our intermediate state the lowest hyperfine level of the

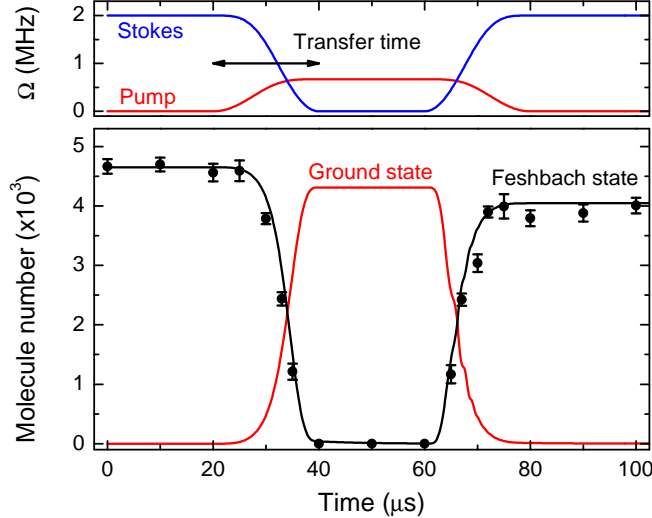


Figure 2: Transfer of molecules to the absolute ground state and back using STIRAP. Top: analytic approximations of the Rabi frequency profiles for the transfer. The maximum values for both the pump and Stokes are both measured (see section 4). Bottom: Population remaining in the initial (Feshbach) state. Circles are experimental data, and show a one-way efficiency of 92(1)%. The black and red lines are a simulation which includes the laser linewidth and has no free parameters, as explained in the text. Note that most of the outward transfer occurs in the last 10  $\mu\text{s}$  of the ramp because of the high Stokes Rabi frequency.

$|\text{}^3\Pi_1, v' = 29, J' = 1\rangle$  rovibrational level, which has high transition strengths to both states and a long excited-state lifetime suitable for STIRAP [27].

We transfer the molecules to the ground state by varying the Rabi frequencies of the pump and Stokes transitions as shown in the upper panel of figure 2. Both lasers are tuned on resonance with the 3-level system. The Stokes beam is initially turned on to 15.2 mW for 20  $\mu\text{s}$ . With  $\Omega_S \neq 0$  and  $\Omega_P = 0$ , the dark state  $|\psi\rangle$  is equivalent to the starting Feshbach state  $|A\rangle$  (see equation 2). The Stokes beam is then ramped down in 20  $\mu\text{s}$  while the pump beam is simultaneously ramped up to 14.5 mW. This adiabatically transfers the population to the ground state  $|B\rangle$ . We cannot detect the ground state directly, so after a 20  $\mu\text{s}$  hold we reverse the process to transfer back to the initial state, allowing measurement of the square of the one-way efficiency. We map out the transfer by truncating the pulse sequence and recording the number of molecules remaining in the state  $|A\rangle$ , as shown in figure 2.

In our previous work we achieved 50% transfer efficiency [26], but this was limited by the presence of the 1550 nm trapping beams, which caused a spatially varying AC Stark shift of the pump transition and reduced the coherence of the pump transition. In this work we switch off the trapping beams for 120  $\mu\text{s}$  during the transfer sequence to remove this effect. The magnetic gradient coil is turned off earlier in the sequence, so during the transfer the molecules are in free flight in a uniform magnetic field of  $\sim 181.624(1)$  G with a curvature of  $0.3 \text{ G cm}^{-2}$ . The optical trap is switched back on after the transfer sequence to recapture the remaining Feshbach molecules. The axial trapping frequency is 180 Hz, which corresponds to a period of 5.5 ms. The molecules do not move significantly while the trap is off for 20  $\mu\text{s}$ , so there is no measureable drop in the number or increase in the temperature. Using this method we observe a one-way transfer efficiency of 92(1)% and create a sample of 4300 ground-state molecules, as seen in figure 2.

We identify the hyperfine ground state we are addressing by changing the polarisation of the Stokes light. The  $|-6(2,4)d(2,4)\rangle$  initial state has  $M_{\text{tot}} = 4$ . The pump laser polarisation is set parallel to the quantisation axis and thus drives  $\pi$  transitions ( $\Delta m = 0$ ) to  $M_{\text{tot}} = 4$  in the excited state. We can set the Stokes polarisations parallel or perpendicular to the quantisation axis, and drive either  $\pi$  ( $\Delta m = 0$ ) or  $\sigma^\pm$  ( $\Delta m = \pm 1$ ) transitions. This lets us address either the  $M_{\text{tot}} = 4$  or  $M_{\text{tot}} = 3, 5$  ground states. In figure 3

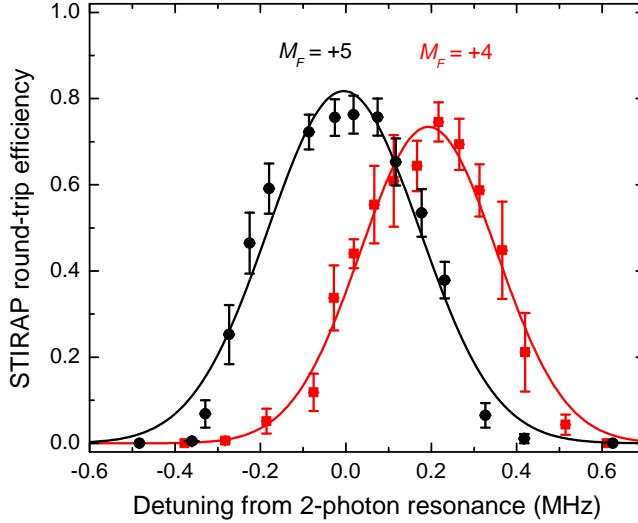


Figure 3: Observation of the ground-state hyperfine splitting. We measure the STIRAP transfer efficiency as the Stokes laser is scanned, and change the polarisation to drive either  $\sigma^\pm$  or  $\pi$  transitions. The states are identified as the  $M_{\text{tot}} = 4$  and  $M_{\text{tot}} = 5$  states indicated in figure 1, and the 0.19 MHz separation between them matches with the predicted splitting. Gaussian fits are shown to guide the eye.

we see the effect of changing the Stokes polarisation. We observe transfer to only two hyperfine states, and the 0.19(1) MHz splitting combined with the selection rules allows us to identify them as the  $M_{\text{tot}} = 4$  and  $M_{\text{tot}} = 5$  states marked with dots in figure 1(b). We have not observed other hyperfine states with  $M_{\text{tot}} = 3$  or 4, and believe this is because the transition strengths to these states are too low. We note that  $M_{\text{tot}} = 5$  is the absolute ground state at 181.6 G.

## 4 Characterising the molecular transitions

The transfer efficiency in equation 3 depends on the Rabi frequencies  $\Omega_P$  and  $\Omega_S$  and the excited-state linewidth  $\Gamma$ . If we wish to model the STIRAP transfer, we must first make reliable measurements of all these parameters.

We measure the transition strengths by driving and directly observing Rabi oscillations on each transition. For an open 2-level system where the excited state decays to other levels at a rate  $\Gamma$ , the probability  $P_A(t)$  of finding the system in the lower state oscillates and decays [38] as

$$P_A(t) = \cos^2\left(\frac{\Omega t}{2}\right) e^{-\Gamma t/2}. \quad (4)$$

We assume here that the “closed” decay rate from the upper to the lower state is negligible. We note the factor of 1/2 in the decay term, which arises because the oscillations mean the system spends only half the time in the excited state. To measure the pump transition, we pulse on 12.4 mW of resonant pump light for a variable time of a few  $\mu\text{s}$  and monitor the population in the initial  $|-6(2,4)d(2,4)\rangle$  state. We see Rabi oscillations driven on the pump transition, as shown in figure 4(a).

To observe the Stokes Rabi frequency, the molecules are first transferred to the ground state by STIRAP. The Stokes beam is then switched on to 3.4 mW for a few  $\mu\text{s}$ , with the pump beam off, before the molecules are transferred back to the Feshbach state by STIRAP. Rabi oscillations on the Stokes transition are shown in figure 4(b).

The simple model of the Rabi oscillations in equation 4 can estimate the Rabi frequency, but gives a poor fit for longer pulse durations. This is because the oscillations begin to dephase at later times due to variation

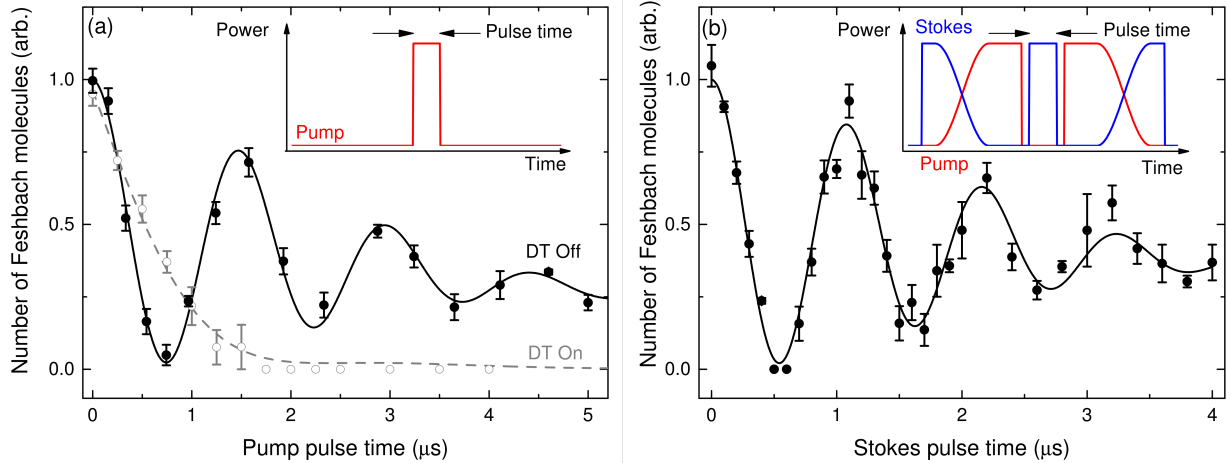


Figure 4: Rabi oscillations on (a) the pump and (b) the Stokes transitions. A fit to each is shown, which includes decay of the excited state and dephasing from spatial variation of the Rabi frequency. Inset are sketches of the pulse sequences for each measurement, with the pump laser in red and the Stokes in blue. For the pump, we show the effect of carrying out the same pulse sequence with the dipole trap (DT) on (grey empty circles) and off (black filled circles). We cannot drive Rabi oscillations in the presence of the dipole trap as explained in the main text. For the Stokes, we transfer the molecules to the ground state by STIRAP before driving the oscillations, and then transfer any remaining ground state population back to the Feshbach state for detection.

in Rabi frequency across the cloud. Daniel *et al.* [39] build an analytic theoretical model including the thermal motion of the sample and Rabi frequencies varying over distances smaller than the imaging resolution. Here the dissociation and detection scheme we use means we can monitor only the total population and cannot resolve variations in the Rabi frequency across the cloud. Rough calculations show the thermal effects are several orders of magnitude too small to be measured in our system, leaving only the dephasing term. This gives an oscillation of the form

$$N = \frac{N_0}{2} e^{-\Gamma t/2} \left( 1 + \exp\left(-\frac{t^2}{T_x^2}\right) \cos(\Omega t) \right), \quad (5)$$

$$T_x = \frac{\sqrt{2}}{\sigma_I \cdot \partial_x \Omega}, \quad (6)$$

where  $T_x$  is the dephasing time from the spatial variation of the Rabi frequency,  $\sigma_I$  is the molecule sample size and  $\partial_x \Omega$  is the Rabi frequency gradient across the sample. Fits to these equations are shown in figure 4 and give pump and Stokes Rabi frequencies of  $2\pi \times 666(6)$  kHz and  $2\pi \times 915(7)$  kHz respectively. The dephasing times are  $3.2(3)$   $\mu$ s and  $2.5(2)$   $\mu$ s respectively. These values are roughly consistent (within a factor of 2) with the expected dephasing time calculated by equation 6, with a transverse cloud size of  $\sim 10$   $\mu$ m exactly at the centre of a 35  $\mu$ m Gaussian beam.

We use our measured beam sizes and powers to calculate reduced Rabi frequencies of  $2\pi \times 0.9(1)$  kHz  $\sqrt{I_P/(\text{mW cm}^{-2})}$  for the pump transition and  $2\pi \times 2.2(2)$  kHz  $\sqrt{I_S/(\text{mW cm}^{-2})}$  for the Stokes. These values have been measured in Innsbruck [27] using the decay time at low Rabi frequency, when  $\Omega \ll \Gamma$  and the Rabi oscillations are not visible. Our values agree well with those measured in Innsbruck, who give values of  $2\pi \times 0.8(2)$  kHz  $\sqrt{I_P/(\text{mW cm}^{-2})}$  and  $2\pi \times 2.8(7)$  kHz  $\sqrt{I_S/(\text{mW cm}^{-2})}$  respectively (see supplementary material for [27]).

The fits in figure 4 also give us the excited-state linewidth. The oscillations on the pump transition, figure 4(a), give a decay rate of  $\Gamma = 2\pi \times 39(4)$  kHz, while the Stokes transition data, figure 4(b), give  $\Gamma = 2\pi \times 24(6)$  kHz. Another identical measurement of the pump transition gave  $\Gamma = 2\pi \times 41(9)$  kHz (data not shown). Our best estimate of the linewidth is a weighted average of these measurements,  $\Gamma = 2\pi \times 35(3)$  kHz, and we use this in our model of the STIRAP transfer (section 5).

The linewidth fitted to the Rabi oscillations is a factor of 4 smaller than that measured from the width of the spectroscopic feature at low power both in our group and in Innsbruck [27]. The reason for this discrepancy is currently unknown, and the uncertainty in the lifetime is currently the least well-characterised factor in our system as both measurement methods have their weaknesses. Measurement of the width of the spectroscopic feature is difficult as the power must be kept low enough not to reduce the molecule number to zero when on resonance. However, using too low a power reduces the signal to noise such that a reliable measurement is not feasible. On the other hand, obtaining the linewidth  $\Gamma$  from Rabi oscillations is problematic because it is difficult to separate  $\Gamma$  from the dephasing time  $T_x$  when fitting the results. For either method, the result shows that we clearly meet the conditions for efficient transfer in equation 3.

From the Rabi frequencies and the intensities of our beams, we calculate transition dipole moments of  $8.1(9) \times 10^{-4} ea_0$  for the pump transition and  $2.0(2) \times 10^{-3} ea_0$  for the Stokes. Using the transition frequencies of 192.572 THz and 384.230 THz respectively, we get decay rates for these transitions of  $\Gamma_P = 2\pi \times 55(6)$  mHz and  $\Gamma_S = 2\pi \times 1.4(1)$  Hz. Since these rates are  $< 10^{-4}$  of the total excited-state linewidth, we conclude that spontaneous decay along the pump and Stokes transitions is negligible compared to decay to other undetectable levels, i.e. the excited state is entirely open.

It is important to note that all our Rabi frequency measurements are carried out in free space. The wavelength of our optical dipole trap is close to that of the pump transition and causes an AC Stark shift of  $\sim 700$  kHz at the  $0.194$  mW  $\mu\text{m}^{-2}$  intensity used in our experiment. This Stark shift varies spatially across the cloud and we calculate that this reduces the dephasing time  $T_x$  to less than  $1 \mu\text{s}$ . Additionally, there may be an increase in off-resonant scattering from the trapping light which reduces the lifetime of the excited state dramatically. The combination of these effects may be seen in the grey open circles of Fig. 4(a) and was the cause of the reduced STIRAP transfer efficiency of  $\sim 50\%$  we have reported previously [26].

## 5 Modelling the transfer

We model the STIRAP transfer using a numerical simulation based on an open three-level ‘‘lambda’’ system, as shown in figure 5. This system has a three-level Hamiltonian (not including decay to state  $|L\rangle$ ):

$$\hat{H} = \frac{\hbar}{2} \begin{pmatrix} 0 & \Omega_P(t) & 0 \\ \Omega_P(t) & 2\Delta_P & \Omega_S(t) \\ 0 & \Omega_S(t) & 2(\Delta_P - \Delta_S) \end{pmatrix}. \quad (7)$$

From this, we construct the Lindblad master equation, and add a term for decay  $|C\rangle \rightarrow |L\rangle$ . To make the transfer, the AOM drivers are modulated by voltage ramps of the form  $V_P(t) = \sin^2(\pi t/2T)$ ,  $V_S(t) = \cos^2(\pi t/2T)$  with a transfer time  $T$ . We analytically approximate the response  $R(V) = \frac{1}{2}(1 - \cos(\pi V))$  of our AOMs and RF amplifiers, and scale  $\Omega(t) = \Omega_0 \sqrt{R(V)}$  for each laser. We initialise the simulation in state  $|A\rangle$ .  $\Omega_0$  is scaled with the powers used in each individual experiment. We use the excited-state lifetime measured from the decay of the oscillations in figure 4. By numerically integrating the master equation using the QuTIP module in Python [40] with 200 ns timesteps, we calculate the population in each of the states through the transfer sequence. We repeat the sequence of  $\Omega_{P,S}$  in reverse to calculate the round-trip efficiency which can be matched to the experiment. The simulated Rabi frequency profile is shown in figure 2.

This basic model of the three-level open system overestimates the transfer efficiency as  $> 99\%$ . In figure 6(a) we vary the length of the transfer ramps. Without noise, the round-trip efficiency approaches 1, but experimentally it drops for transfer ramps longer than  $\sim 50 \mu\text{s}$ .

We account for the lower transfer efficiency by adding the effects of laser linewidth and noise. The transfer efficiency is relatively insensitive to the 2-photon detuning, so we consider only the simplified case where the

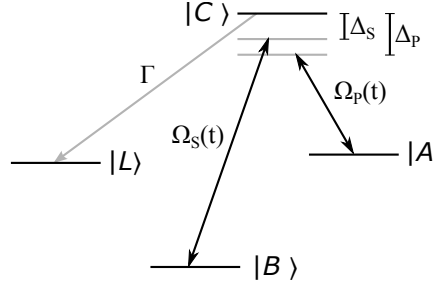


Figure 5: Level system for modelling STIRAP transfer to the ground state.  $|A\rangle$  is the initial Feshbach state,  $|B\rangle$  is the final ground state, and  $|C\rangle$  is the lossy intermediate state which decays to many undetectable states represented by  $|L\rangle$ .  $\Omega_{P,S}(t)$  are the pump and Stokes Rabi frequencies, and  $\Delta_{P,S}(t)$  are the detunings.

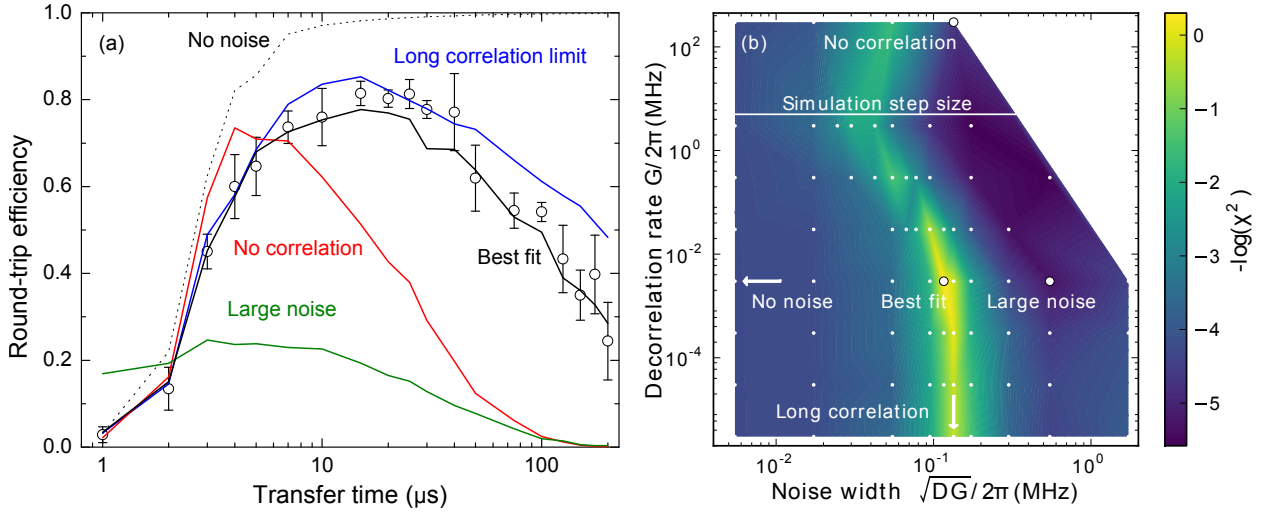


Figure 6: Effect of laser noise on STIRAP transfer. (a) Efficiency of STIRAP transfer as the ramp speed is varied. Experimental data are shown with  $1\sigma$  standard errors. Monte Carlo simulations are shown for several different values of the laser decorrelation rate  $G$  and laser noise amplitude  $\sqrt{DG}$ , as explained in the text. The apparent efficiency for the green “large noise” curve at short times is from molecules remaining in the initial state, i.e. the transfer fails. (b)  $\chi^2$  goodness-of-fit contour plot for the data and model in panel (a). White dots are the values we have simulated. We indicate the parameters matching the curves in panel (a), and arrows denote limiting cases. Note the long ridge of good fits spanning several orders of magnitude in correlation time, approaching the long-correlation limit where a single frequency is randomly selected for each experimental shot or simulation run.

laser noise is uncorrelated but identical for both lasers. We do this by replacing the detuning  $\Delta_{\text{P,S}}$  with time-varying functions, following Yatsenko *et al.* [31]:

$$\Delta_{\text{P,S}} \rightarrow \Delta_{\text{P,S}} + \xi(t), \quad (8)$$

where  $\xi(t)$  is some zero-mean random process. By averaging over many simulations with randomised  $\xi(t)$ , we get the average transfer efficiency and populations through the transfer process. Yatsenko *et al.* [31] suggest a model using exponentially correlated coloured noise:

$$\xi(t + \Delta t) = \xi(t)e^{-G\Delta t} + h(t), \quad (9)$$

where  $h(t)$  is a random Gaussian variable with second moment  $DG(1 - e^{-2G\Delta t})$ .  $G$  is the inverse phase correlation time of the laser field, while  $D$  is the phase diffusion coefficient, giving a noise amplitude of  $\sqrt{DG}$ .

We test this noise model in figure 6(a). This shows the effect of the phase correlations, with an uncorrelated model in red, a partially correlated model in black which gives the best fit to the data, and a perfectly correlated model in blue which overestimates the transfer efficiency for all transfer times. We also show in green the effect of increasing the total noise amplitude at the same correlation time as the best fit, so that the laser is often far off resonance and the molecules never leave the initial state.

In figure 6(b) we estimate the values of  $D$  and  $G$  with the  $\chi^2$  goodness-of-fit to the experimental data in figure 6(a). The best fit occurs at a phase correlation time of around 300  $\mu\text{s}$ , which corresponds to a short-term laser linewidth of  $G \sim 2\pi \times 3$  kHz. Measurements from delayed self-heterodyne interferometry [32] estimated the laser linewidth as  $2\pi \times 0.5$  kHz. These are consistent, as we note that the best-fit point is remarkably insensitive to the phase correlation time, with only an order-of-magnitude estimate possible. We see this as the long vertical ‘‘ridge’’ of good fits in figure 6(b). However, the noise amplitude  $\sqrt{DG}$  is much more sensitive, and we fit  $\sqrt{DG} \sim 2\pi \times 130$  kHz, also consistent with our measurements of the shot-to-shot stability of our laser frequency [32]. In our case, where the correlation time is much longer than the transfer time, the frequency noise is effectively a nearly constant detuning, which matches with slow, shot-to-shot noise variation in the laser frequency.

We estimate the sensitivity of the transitions to magnetic field fluctuation. The theoretical results in figure 1(a) and (b) give Zeeman shifts of 2.22 MHz  $\text{G}^{-1}$  for the Feshbach state and 4.05 kHz  $\text{G}^{-1}$  for ground state. We have measured the Zeeman shift of the excited state as 0.4(2) MHz  $\text{G}^{-1}$ . Using these gradients, we estimate the shot-to-shot frequency noise above corresponds to a field stability of  $\pm 60$  mG for the pump transition, or  $\pm 260$  mG for the Stokes. The former is within our measured field reproducibility over many weeks [36], though we have no way to measure the field stability on a shot-to-shot basis. Thus field fluctuations are a possible limitation on the transfer efficiency.

We test the model further by comparing it to the transfer in figure 2. We use the measured Rabi frequencies and the best-fit values of  $D$  and  $G$  from figure 6, so that the model has no free parameters. We average over 200 runs of the simulation to generate the Feshbach and ground-state populations. The model has a reduced  $\chi^2$  of 3.5, with the deviations coming mainly from the transfer portions of the graph, indicating the model does not reproduce the transfer perfectly, probably due to errors in the simulated Rabi frequency profile. However, it is clear that the model is a reasonable description of the transfer.

## 6 Conclusions

In this paper, we presented transfer of  $^{87}\text{RbCs}$  Feshbach molecules to the ground state using STIRAP. We reached 92(1)% transfer efficiency and created over 4000 ground-state molecules. We fully characterised the transfer route with direct measurements of the Rabi frequencies, which were consistent with previous work. We also measured the excited-state lifetime and found it a factor of four longer than previous work. We modelled the transfer including a Monte Carlo model of the laser noise. We found the main limitation to the transfer efficiency is shot-to-shot noise, rather than laser coherence, and these were consistent with previous independent measurements of the laser noise.

This work demonstrates a relatively easy and reliable method for transfer of molecules to the absolute ground state, and paves the way for exciting experiments in quantum-controlled chemistry [10, 11] and controllable quantum many-body physics in the strongly interacting regime [24]. Since this work, we have captured the ground-state molecules after the transfer, and we are now investigating the loss processes in long-lived samples of highly polar molecules. We are currently building a new optical trap at 1064 nm, which should allow the transfer with fully trapped molecules and loading into a lattice potential. From here we intend to investigate the formation of long-lived collision complexes and the effect of the electric dipole moment on scattering rates, to test the collisional stability of nonreactive  $^{87}\text{RbCs}$  molecules [41].

## 7 Acknowledgments

We would like to thank T. Ogden for his help in developing the STIRAP simulation, M. Köppinger, Z. Ji and B. Lu for their contributions in the earlier stages of this project, and J. Aldegunde for calculations of the ground-state hyperfine structure. This work was supported by the U.K. Engineering and Physical Sciences Research Council (EPSRC) Grants No. EP/H003363/1, EP/I012044/1 and GR/S78339/01, and by European Office of Aerospace Research and Development (EOARD) Grant No. FA8655-10-1-3033. The data presented in this paper are available at DOI:10.15128/r1xp68kg20n.

## References

- [1] L. D. Carr, D. Demille, R. V. Krems, and J. Ye. Cold and ultracold molecules: science, technology and applications. *New J. Phys.*, 11(5):055049, 2009.
- [2] D.S. Jin and J. Ye. Introduction to ultracold molecules: New frontiers in quantum and chemical physics. *Chem. Rev.*, 112(9):4801–4802, 2012.
- [3] M. Lemesko, R. V. Krems, J. M. Doyle, and S. Kais. Manipulation of molecules with electromagnetic fields. *Mol. Phys.*, 111(12-13):1648–1682, 2013.
- [4] D. DeMille. Quantum computation with trapped polar molecules. *Phys. Rev. Lett.*, 88:067901, Jan 2002.
- [5] L. Santos, G. V. Shlyapnikov, P. Zoller, and M. Lewenstein. Bose-einstein condensation in trapped dipolar gases. *Phys. Rev. Lett.*, 85:1791–1794, Aug 2000.
- [6] M. A. Baranov, M. Dalmonte, G. Pupillo, and P. Zoller. Condensed matter theory of dipolar quantum gases. *Chemical Reviews*, 112(9):5012–5061, 2012.
- [7] V. V. Flambaum and M. G. Kozlov. Enhanced sensitivity to the time variation of the fine-structure constant and  $m_p/m_e$  in diatomic molecules. *Phys. Rev. Lett.*, 99:150801, Oct 2007.
- [8] T. A. Isaev, S. Hoekstra, and R. Berger. Laser-cooled raf as a promising candidate to measure molecular parity violation. *Phys. Rev. A*, 82:052521, Nov 2010.
- [9] J. J. Hudson, D. M. Kara, I. J. Smallman, B. E. Sauer, M. R. Tarbutt, and E. A. Hinds. Improved measurement of the shape of the electron. *Nature*, 473(7348):493–496, 2011.
- [10] S. Ospelkaus, K.-K. Ni, D. Wang, M. H. G. de Miranda, B. Neyenhuis, G. Quéméner, P. S. Julienne, J. L. Bohn, D. S. Jin, and J. Ye. Quantum-state controlled chemical reactions of ultracold potassium-rubidium molecules. *Science*, 327(5967):853–857, 2010.
- [11] R. V. Krems. Cold controlled chemistry. *Phys. Chem. Chem. Phys.*, 10:4079–4092, 2008.
- [12] J. F. Barry, D. J. McCarron, E. B. Norrgard, M. H. Steinecker, and D. DeMille. Magneto-optical trapping of a diatomic molecule. *Nature*, 512(7514):286–289, 2014.

- [13] D. J. McCarron, E. B. Norrgard, M. H. Steinecker, and D. DeMille. Improved magneto-optical trapping of a diatomic molecule. *New J. Phys.*, 17(3):035014, 2015.
- [14] V. Zhelyazkova, A. Cournol, T. E. Wall, A. Matsushima, J. J. Hudson, E. A. Hinds, M. R. Tarbutt, and B. E. Sauer. Laser cooling and slowing of caF molecules. *Phys. Rev. A*, 89:053416, May 2014.
- [15] R. Glöckner, A. Prehn, B. G. U. Englert, G. Rempe, and M. Zeppenfeld. Rotational cooling of trapped polyatomic molecules. *Phys. Rev. Lett.*, 115:233001, Dec 2015.
- [16] M. Zeppenfeld, B. G. U. Englert, R. Glöckner, A. Prehn, M. Mielenz, C. Sommer, L. D. van Buuren, M. Motsch, and G. Rempe. Sisyphus cooling of electrically trapped polyatomic molecules. *Nature*, 491(7425):570–573, November 2012.
- [17] T. Köhler, K. Góral, and P. S. Julienne. Production of cold molecules via magnetically tunable feshbach resonances. *Rev. Mod. Phys.*, 78:1311–1361, Dec 2006.
- [18] C. Chin, R. Grimm, P. Julienne, and E. Tiesinga. Feshbach resonances in ultracold gases. *Rev. Mod. Phys.*, 82:1225–1286, Apr 2010.
- [19] K. Bergmann, H. Theuer, and B. W. Shore. Coherent population transfer among quantum states of atoms and molecules. *Rev. Mod. Phys.*, 70:1003–1025, Jul 1998.
- [20] Johann G. Danzl, Elmar Haller, Mattias Gustavsson, Manfred J. Mark, Russell Hart, Nadia Bouloufa, Olivier Dulieu, Helmut Ritsch, and Hanns-Christoph Nägerl. Quantum gas of deeply bound ground state molecules. *Science*, 321(5892):1062–1066, 2008.
- [21] J. G. Danzl, M. J. Mark, E. Haller, M. Gustavsson, R. Hart, J. Aldegunde, J. M. Hutson, and H.-C. Nägerl. An ultracold high-density sample of rovibronic ground-state molecules in an optical lattice. *Nat. Phys.*, 6:265, 2010.
- [22] F. Lang, K. Winkler, C. Strauss, R. Grimm, and J. Hecker Denschlag. Ultracold triplet molecules in the rovibrational ground state. *Phys. Rev. Lett.*, 101:133005, Sep 2008.
- [23] B. Yan, S. A. Moses, B. Gadway, J. P. Covey, K. R. A. Hazzard, A. M. Rey, D. S. Jin, and J. Ye. Observation of dipolar spin-exchange interactions with lattice-confined polar molecules. *Nature*, 501(7468):521–525, September 2013.
- [24] K. R. A. Hazzard, B. Gadway, M. Foss-Feig, B. Yan, S. A. Moses, J. P. Covey, N. Y. Yao, M. D. Lukin, J. Ye, D. S. Jin, and A. M. Rey. Many-body dynamics of dipolar molecules in an optical lattice. *Phys. Rev. Lett.*, 113:195302, Nov 2014.
- [25] K.-K. Ni, S. Ospelkaus, D. Wang, G. Quéméner, B. Neyenhuis, M. H. G. de Miranda, J. L. Bohn, J. Ye, and D. S. Jin. Dipolar collisions of polar molecules in the quantum regime. *Nature*, 464(7293):1324–1328, 2010.
- [26] P. K. Molony, P. D. Gregory, Z. Ji, B. Lu, M. P. Köppinger, C. R. Le Sueur, C. L. Blackley, J. M. Hutson, and S. L. Cornish. Creation of ultracold  $^{87}\text{Rb}^{133}\text{Cs}$  molecules in the rovibrational ground state. *Phys. Rev. Lett.*, 113:255301, Dec 2014.
- [27] T. Takekoshi, L. Reichsöllner, A. Schindewolf, J. M. Hutson, C. R. Le Sueur, O. Dulieu, F. Ferlaino, R. Grimm, and H.-C. Nägerl. Ultracold dense samples of dipolar RbCs molecules in the rovibrational and hyperfine ground state. *Phys. Rev. Lett.*, 113:205301, Nov 2014.
- [28] J. W. Park, Sebastian A. Will, and M. W. Zwierlein. Ultracold dipolar gas of fermionic  $^{23}\text{Na}^{40}\text{K}$  molecules in their absolute ground state. *Phys. Rev. Lett.*, 114:205302, May 2015.
- [29] M. Guo, B. Zhu, B. Lu, X. Ye, F. Wang, R. Vexiau, N. Bouloufa-Maafa, G. Quéméner, O. Dulieu, and D. Wang. arXiv:1602.03947 [cond-mat.quant-gas], 2016.

- [30] J. R. Kuklinski, U. Gaubatz, F. T. Hioe, and K. Bergmann. Adiabatic population transfer in a three-level system driven by delayed laser pulses. *Phys. Rev. A*, 40:6741–6744, Dec 1989.
- [31] L. P. Yatsenko, V. I. Romanenko, B. W. Shore, and K. Bergmann. Stimulated raman adiabatic passage with partially coherent laser fields. *Phys. Rev. A*, 65:043409, Apr 2002.
- [32] P. D. Gregory, P. K. Molony, M. P. Köppinger, A. Kumar, Z. Ji, B. Lu, A. L. Marchant, and S. L. Cornish. A simple, versatile laser system for the creation of ultracold ground state molecules. *New J. Phys.*, 17(5):055006, 2015.
- [33] M. L. Harris, P. Tierney, and S. L. Cornish. Magnetic trapping of a cold Rb-Cs atomic mixture. *J. Phys. B*, 41(3):035303, 2008.
- [34] D. J. McCarron, H. W. Cho, D. L. Jenkin, M. P. Köppinger, and S. L. Cornish. Dual-species bose-einstein condensate of  $^{87}\text{Rb}$  and  $^{133}\text{Cs}$ . *Phys. Rev. A*, 84:011603, Jul 2011.
- [35] H. W. Cho, D. J. McCarron, D. L. Jenkin, M. P. Köppinger, and S. L. Cornish. A high phase-space density mixture of  $^{87}\text{Rb}$  and  $^{133}\text{Cs}$ : towards ultracold heteronuclear molecules. *EPJ D*, 65(1-2):125–131, 2011.
- [36] M. P. Köppinger, D. J. McCarron, D. L. Jenkin, P. K. Molony, H.-W. Cho, S. L. Cornish, C. R. Le Sueur, C. L. Blackley, and J. M. Hutson. Production of optically trapped  $^{87}\text{RbCs}$  feshbach molecules. *Phys. Rev. A*, 89:033604, Mar 2014.
- [37] E. D. Black. An introduction to pound-drever-hall laser frequency stabilization. *Am. J. Phys.*, 69(1):79–87, 2001.
- [38] N. Kosugi, S. Matsuo, K. Konno, and N. Hatakenaka. Theory of damped rabi oscillations. *Phys. Rev. B*, 72:172509, Nov 2005.
- [39] A. Daniel, R. Agou, O. Amit, D. Groswasser, Y. Japha, and R. Folman. Damping of local rabi oscillations in the presence of thermal motion. *Phys. Rev. A*, 87:063402, Jun 2013.
- [40] J.R. Johansson, P.D. Nation, and F. Nori. Qutip 2: A python framework for the dynamics of open quantum systems. *Comput. Phys. Commun.*, 184(4):1234 – 1240, 2013.
- [41] Michael Mayle, Goulven Quéméner, Brandon P. Ruzic, and John L. Bohn. Scattering of ultracold molecules in the highly resonant regime. *Phys. Rev. A*, 87:012709, Jan 2013.